Range of validity and intermittent dynamics of the phase of oscillators with nonlinear self-excitation

D.V. Strunin[1] and M.G. Mohammed

Computational Engineering and Science Research Centre,

Faculty of Health, Engineering and Sciences, University of Southern Queensland,

Toowoomba, QLD 4350, Australia

Abstract

A range of active systems, particularly of chemical nature, are known to perform self-excited oscillations coupled by diffusion. The role of the diffusion is not trivial so that the differences in the phase of the oscillations through space may persist, depending on the values of the controlling parameters of the system. Firstly, we analyse a 6th-order nonlinear partial differential equation describing such dynamics. We evaluate the range of the parameters leading to different finite versions of the equation, specifically a version based on nonlinear excitation and a version based on linear excitation. In the second part of the work we solve the equation in two spatial dimensions by finite-difference discretization in space and subsequent numerical integration of a system of ordinary differential equations in time. A forced variant of the equation is derived and selected exact solutions are presented. They are also used to verify the numerical code. For the unforced equation, irregular dynamics intermitting with periods of slow evolution are recorded and discussed.

Key words: Active dissipative system, nonlinear excitation, parametric space, irregular dynamics

1 Introduction

In this work we analyse oscillators representing a class of dissipative active systems with self-excitation. As examples of such systems mention fronts of gasless combustion [1, 2], certain

[1]corresponding author, email: strunin@usq.edu.au, tel.: +61-7-4631-5541, fax: +61-7-4631-5550

type of reaction-diffusion systems [3, 4, 5] and seismic waves in fluid-saturated rocks [6]. Intuitively, diffusion (or thermal conductivity) should smooth out the differences of the phase of the oscillations in space. However, as is now well-understood [1, 3], the combined effect of the diffusion and self-excitation may produce complicated dynamics, during which the difference may persist as time goes. Earlier we derived [7, 8, 9] a form of such an equation based on *nonlinear* self-excitation,

$$\partial_t u = -A\nabla^2 u(\nabla u)^2 + B(\nabla u)^4 + C\nabla^6 u\,, \tag{1}$$

where $A > 0$ and $C > 0$. The former condition guarantees that the term, $-A\nabla^2 u(\nabla u)^2$, acts as a nonlinear excitation (the anti-diffusion, $-D\nabla^2 u$, with the nonlinear diffusion coefficient, $D = A(\nabla u)^2$), and the latter condition ensures dissipative effect of the term $C\nabla^6 u$. We will refer to (1) as the nonlinearly excited phase (NEP) equation.

Clearly, (1) has the trivial, spatially-uniform solution

$$u = \text{const}\,.$$

It is stable to small perturbations since the linearized form of the equation is dissipative to all wavelengths,

$$\partial_t u = C\nabla^6 u\,.$$

Therefore, in order to kick-start self-sustaining dynamics one needs a sufficiently strong initial perturbation. If, at some stage of the dynamics, the surface $u(x, y, t)$ flattens out to significant extent, the motion will decay forever.

Previously we solved equation (1) in 1D numerically, using Galerkin method, under periodic boundary conditions [7]. A settled regime was obtained, in which a kink-shaped wave moves along a spiral trajectory on the surface of a cylinder (see graph (b)). Such a regime profoundly resembles an experimentally observed spinning combustion wave [2], illustrated on the photo. It is important that it is not just the correct shape – a kink – of the wave that is reproduced but also the dynamic mechanism behind it. In a laboratory, the spinning combustion occurs when the reacting chemical composition is diluted with some neutral admixture. As a consequence, it becomes difficult for the combustion process to maintain itself (it actually occurs on the brink of collapse). As a result, the front has to form a cavity

(a) A post-combustion trace left by the spinning solid flame on a hollow cylinder; courtesy of A.G. Strunina (see also similar photos and discussions in [2, 10]).

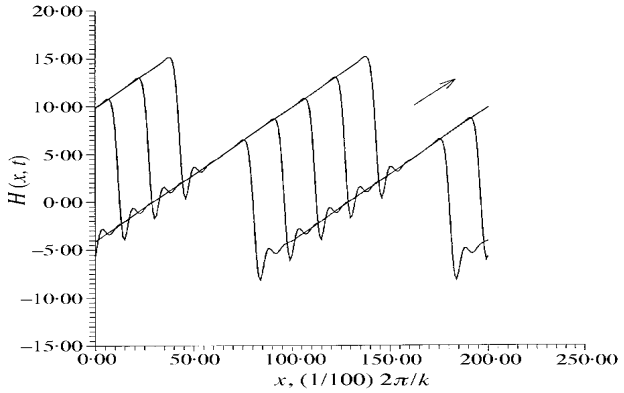

(b) A running spinning wave solution of Eq. (1) (five successive shapes) evolved from a randomly chosen initial condition [7].

Figure 1: Comparison of the experiment and simulation.

(kink) of certain size and moving with certain velocity, where the cold unburned composition is surrounded from two sides by the hot reaction products. This is the only way the combustion can survive under the "difficult" conditions. For the 1D topology we did not investigate whether, apart from the periodic waves, there may also realise irregular regimes. Perhaps, those are possible at large diameters of the cylinder, when there is enough space for a number of kinks to co-exist interact with each other in a complicated way. For the 2D topology, that is with an extra dimension available, we have a strong anticipation that complicated, possibly chaotic, dynamics may indeed form and self-sustain provided the size of the space domain is sufficiently large.

Another area of application of the equation (1) are reaction-diffusion systems, in particular those exhibiting nonlocal effects. For such systems equation (1) was derived [9] by a rigorous procedure as a truncated version of the following infinite (also referred to as generalized) phase diffusion equation,

$$\begin{aligned}\partial_t u = {} & a_1\nabla^2 u + a_2(\nabla u)^2 + \\ & b_1\nabla^4 u + b_2\nabla^3 u\nabla u + b_3(\nabla^2 u)^2 + b_4\nabla^2 u(\nabla u)^2 + b_5(\nabla u)^4 + \\ & g_1\nabla^6 u + g_2\nabla^5 u\nabla u + g_3\nabla^4 u\nabla^2 u + g_4(\nabla^3 u)^2 + g_5\nabla^4 u(\nabla u)^2 + \dots .\end{aligned} \tag{2}$$

Here u denotes the phase of oscillations, and a_n, b_n, g_n, e_n, ... are constant coefficients. The right-hand side of (2) is virtually a Taylor series in small parameter $\nabla^2 \sim (1/L)^2$, with L standing for the typical length scale, presumed large. There may be different kinds of balance between the terms in (2) depending on the magnitudes and signs of the coefficients. For example, when $a_1 > 0$ and the initial field $u(x, y, 0)$ is sufficiently smooth, the diffusion term dominates during the entire period of evolution. The equation is effectively reduced to the linear diffusion equation

$$\partial_t u = a_1 \nabla^2 u \,. \tag{3}$$

In the case $a_1 = -\varepsilon < 0$ (assumed small) and, by the order of magnitude, $a_2 = 1$, $b_1 = -1$, equation (2) reduces to the Kuramoto–Sivashinsky (KS) equation [1, 3],

$$\partial_t u = -\varepsilon \nabla^2 u + (\nabla u)^2 - \nabla^4 u \,. \tag{4}$$

The KS equation contains the *linear* anti-diffusion term, $-\varepsilon\nabla^2 u$, which represents excitation; it is counterbalanced by the dissipative term, $-\nabla^4 u$. Taking into account smallness of ε, it is straightforward to show that the scales of u and L resulting from the balance are such that the rest of the terms in (2) are negligible compared to the three balancing terms in (4). In a similar way equation (2) effectively reduces to the finite form (1) when $b_4 = -\varepsilon$ and, by the order, $b_5 = 1$ and $g_1 = 1$ and, additionally, all the lower-order terms in the right-hand side of (2) are negligibly small. To meet this latter condition, the five coefficients a_1, a_2, b_1, b_2 and b_3 (alongside with the coefficient b_4) must be small. Denoting the characteristic scale of the phase variations by $U > 0$ we evaluate in absolute value: $\nabla^2 u(\nabla u)^2 \sim U^3/L^4$, $(\nabla u)^4 \sim U^4/L^4$ and $\nabla^6 u \sim U/L^6$. The balance between the three terms of (1),

$$\varepsilon U^3/L^4 \sim U^4/L^4 \sim U/L^6 \,, \tag{5}$$

governs the scales of the dissipative structures,

$$U \sim \varepsilon \,, \quad L \sim (1/\varepsilon)^{3/2} \,. \tag{6}$$

The smallness condition for the five mentioned coefficients may indeed realize in certain systems and, as we show in the next section, is not a rare occasion. An example is the following system [9],

$$\partial_t \mathbf{X} = \mathbf{f}(\mathbf{X}) + \delta\nabla^2 \mathbf{X} + k_1 \mathbf{g}_1(S_1) + k_2 \mathbf{g}_2(S_2) \,, \tag{7}$$

$$\tau_1 \partial_t S_1 = -S_1 + D\nabla^2 S_1 + h_1(\mathbf{X})\,, \tag{8}$$

$$\tau_2 \partial_t S_2 = -S_2 + D\nabla^2 S_2 + h_2(\mathbf{X})\,. \tag{9}$$

Here δ, k_1, k_2, τ_1, τ_2 and D are constants, and $\mathbf{X}$, S_1 and S_2 represent the concentrations of reactants. This system is relevant to certain type of bio-systems [4]. Equations (7)–(9) leads to a Ginzburg-Landau (GL) equation for the complex amplitude A – measure of the concentrations – with two nonlocal terms,

$$\partial_t A = \mu\sigma A - \beta|A|^2 A + \delta\nabla^2 A$$

$$+k_1\eta_1{}' \int d\mathbf{r}' G_1(\mathbf{r}-\mathbf{r}')A(\mathbf{r}',t) + k_2\eta_2{}' \int d\mathbf{r}' G_2(\mathbf{r}-\mathbf{r}')A(\mathbf{r}',t)\,, \tag{10}$$

where G_n are coupling functions resulting from the presence of chemicals S_1 and S_2. In one dimension,

$$G_n(x) = \frac{1}{2}(\zeta_n + i\eta_n)e^{-(\zeta_n + i\eta_n)|x|}\,, \quad n = 1, 2\,, \tag{11}$$

with

$$\zeta_n = \left(\frac{1+\sqrt{1+\theta_n^2}}{2D}\right)^{1/2}\,,\ \eta_n = \left(\frac{-1+\sqrt{1+\theta_n^2}}{2D}\right)^{1/2}\,. \tag{12}$$

All the new parameters appearing in (10)–(12) are constants. Rescaling (10) (we refer to [4] and [9] for details) leads to

$$\begin{aligned}\partial_t A = {} & A - (1+ic_2)|A|^2 A + (\delta_1 + i\delta_2)\nabla^2 A \\ & +K_1(1+ic_{11})\int dr' G_1(\mathbf{r}-\mathbf{r}')[A(\mathbf{r}') - A(\mathbf{r})] \\ & +K_2(1+ic_{12})\int dr' G_2(\mathbf{r}-\mathbf{r}')[A(\mathbf{r}') - A(\mathbf{r})]\,.\end{aligned} \tag{13}$$

Equation (13) contains 9 independent parameters: δ_1, δ_2, c_{11}, c_{12}, c_2, K_1, K_2, θ_1 and θ_2. The complex amplitude A is connected to the real-valued amplitude, a, and real-valued phase of the oscillations, φ, via

$$A = ae^{-i\varphi}\,. \tag{14}$$

Substituting (14) into the Ginzburg-Landau equation (13) and separating real and imaginary parts, we obtain

$$\partial_t a = a - a^3 + \delta_1\nabla^2 a - \delta_1\, a(\nabla\varphi)^2 + 2\delta_2\nabla a\nabla\varphi + \delta_2\, a\nabla^2\varphi + \mathrm{Re}\, I\,. \tag{15}$$

$$\partial_t\varphi = c_2a^2 + 2\delta_1\frac{\nabla a\nabla\varphi}{a} + \delta_1\nabla^2\varphi - \delta_2\frac{\nabla^2 a}{a} + \delta_2(\nabla\varphi)^2 - \frac{1}{a}\mathrm{Im}\, I\,, \tag{16}$$

where

$$I = \frac{I_0}{e^{-i\varphi}}\,, \tag{17}$$

and I_0 denotes the nonlocal terms in (13).

The real amplitude, a, tends towards 1, driven by $\partial_t a \approx a - a^3$. Note that the terms following $a-a^3$ in (15) are relatively small due to the slow variations in space. Despite being small, they make the amplitude a deviate from 1. At the same time the phase increases at an approximately constant rate as $\varphi = c_2 t$, because the amplitude is approximately driven by $\partial_t\varphi \approx c_2a^2 \approx c_2$. However, being perturbed by the rest of the terms in (16), the phase deviates from c_2t. We define the phase deviation, u, via

$$\varphi = c_2t + u\,. \tag{18}$$

For the slow spatial variations under consideration, $\nabla \sim 1/L \sim \varepsilon_1$ is small. To provide consistency with (6) we state

$$\varepsilon_1 = \varepsilon^{3/2}\,. \tag{19}$$

This relation connects the small parameter ε (our choice), representing the coefficient b_4, with the size of the formed dissipative structures, ε_1 (the consequence of this choice). Thus, the variations of the amplitude and phase are slow because the coefficient b_4 is small. We came to a typical centre manifold situation in which there is a fast variable, a, and a slow variable, φ. The centre manifold theory states that there exists a manifold to which the dynamics are attracted exponentially quickly,

$$a = a[\nabla\varphi]\,. \tag{20}$$

Equation (20) manifests a stiff connection between the amplitude and phase on the centre manifold. This link makes it possible to eliminate the amplitude from (16) and obtain a closed equation for the phase. It is convenient to rescale the variables, $t_1 = \varepsilon_1^2 t$ and $x_1 = \varepsilon_1 x$, so that

$$\nabla = \varepsilon_1\nabla_1\,, \quad \partial_t = \varepsilon_1^2\partial_{t_1}\,. \tag{21}$$

We expand the amplitude into the series in ε_1,

$$a = 1 + \varepsilon_1^2a_2 + \varepsilon_1^4a_4 + \varepsilon_1^6a_6 + \dots\,. \tag{22}$$

Using (21), (18) and (22) in the phase equation (16) and the amplitude equation (15), we derive, for the phase departure introduced in (18),

$$\begin{aligned}
&\varepsilon_1^2\partial_{t_1}u = 2c_2\,\varepsilon_1^2\,a_2 + 2c_2\,\varepsilon_1^4\,a_4 + c_2\,\varepsilon_1^4\,a_2^2 + 2c_2\,\varepsilon_1^6\,a_6\\
&+2\delta_1\,\varepsilon_1^4\,\nabla_1 a_2\nabla_1 u + \delta_1\,\varepsilon_1^2\,\nabla_1^2 u - \delta_2\,\varepsilon_1^4\,\nabla_1^2 a_2 - \delta_2\,\varepsilon_1^6\,\nabla_1^2 a_4\\
&+\delta_2\,\varepsilon_1^2\,(\nabla_1 u)^2 - \frac{1}{a}\mathrm{Im}\,I + \dots
\end{aligned} \tag{23}$$

and, for the amplitude,

$$\begin{aligned}
&\varepsilon_1^4\partial_{t_1}a_2 + \varepsilon_1^6\partial_{t_1}a_4 + \dots = -2\varepsilon_1^2 a_2 - \varepsilon_1^4\left(2a_4 + 3a_2^2\right) - \varepsilon_1^6\left(2a_6 + 6a_2a_4 + a_2^3\right)\\
&+\delta_1\varepsilon_1^2\left(\varepsilon_1^2\nabla_1^2 a_2 + \varepsilon_1^4\nabla_1^2 a_4 + \dots\right) - \delta_1\left(1 + \varepsilon_1^2 a_2 + \varepsilon_1^4 a_4 + \dots\right)\varepsilon_1^2(\nabla_1 u)^2\\
&+2\delta_2\varepsilon_1\left(\varepsilon_1^2\nabla_1 a_2 + \varepsilon_1^4\nabla_1 a_4 + \dots\right)\varepsilon_1\nabla_1 u\\
&+\delta_2\left(1 + \varepsilon_1^2 a_2 + \varepsilon_1^4 a_4 + \dots\right)\varepsilon_1^2\nabla_1^2 u + \mathrm{Re}\,I\,.
\end{aligned} \tag{24}$$

Collecting terms $\sim \varepsilon_1^2$ in (24) we obtain

$$0 = -2a_2 - \delta_1(\nabla_1 u)^2 + \delta_2\nabla_1^2 u + (\mathrm{Re}\,I)_2\,, \tag{25}$$

where $(\mathrm{Re}\,I)_2$ denotes the coefficient at ε_1^2 in the ε_1-series for $\mathrm{Re}\,I$. After the necessary manipulations using the expression I (we refer to [9] for details) we obtain a_2 in terms of $\nabla_1 u$ in the form

$$a_2 = \alpha_1\nabla_1^2 u - \alpha_2(\nabla_1 u)^2\,.$$

Similarly, we find other a_n in terms of $\nabla_1 u$, substitute them into (23) and, after doing necessary algebra, eventually arrive at the phase equation of the form (2). We present it below in two parts. First we give the phase equation following from the Ginzburg-Landau equation with only *one* nonlocal term. Then we explain how it should be transformed in

order to represent the case with *two* nonlocal terms.

$$
\begin{aligned}
\partial_t u = \quad & \nabla^2 u \left[2c_2\alpha_1 + \delta_1 + \frac{K}{4}(\zeta - c_1\eta)C_2 - \frac{K}{4}(c_1\zeta + \eta)S_2 \right] \\
& + (\nabla u)^2 \left[-2c_2\alpha_2 + \delta_2 + \frac{K}{4}(c_1\zeta + \eta)C_2 - \frac{K}{4}(\zeta - c_1\eta)S_2 \right] \\
& + \nabla^4 u \left[2c_2\beta - \delta_2\alpha_1 + \frac{K}{48}(\eta + c_1\zeta)S_4 + \frac{K}{48}(\zeta - c_1\eta)C_4 \right. \\
& \qquad \left. - \frac{K}{4}(\eta + c_1\zeta)C_2\alpha_1 + \frac{K}{4}(\zeta - c_1\eta)S_2\alpha_1 \right] \\
& + \nabla u \nabla^3 u \left[2c_2\beta_2 + 2\delta_1\alpha_1 + 2\delta_2\alpha_2 - \frac{K}{12}(\zeta - c_1\eta)S_4 \right. \\
& \qquad \left. + \frac{K}{12}(\eta + c_1\zeta)C_4 - \frac{K}{2}(\zeta - c_1\eta)S_2\alpha_2 + \frac{K}{2}(\eta + c_1\zeta)C_2\alpha_2 \right] \\
& + \left(\nabla^2 u\right)^2 \left[2c_2\beta_1 + 2c_2\alpha_1^2 + 2\delta_2\alpha_2 - \frac{K}{16}(\zeta - c_1\eta)S_4 \right. \\
& \qquad \left. + \frac{K}{16}(\eta + c_1\zeta)C_4 - \frac{K}{2}(\zeta - c_1\eta)S_2\alpha_2 + \frac{K}{2}(\eta + c_1\zeta)C_2\alpha_2 \right] \\
& + \nabla^2 u (\nabla u)^2 \left[2c_2\beta_3 - 4c_2\alpha_1\alpha_2 - 4\delta_1\alpha_2 - \frac{K}{8}(\zeta - c_1\eta)C_4 - \frac{K}{8}(\eta + c_1\zeta)S_4 \right] \\
& + (\nabla u)^4 \left[2c_2\beta_4 + 2c_2\alpha_2^2 + \frac{K}{48}(\zeta - c_1\eta)S_4 - \frac{K}{48}(\eta + c_1\zeta)C_4 \right] \\
& + \nabla^6 u \left[2c_2 \left(\frac{1}{2}\delta_1\beta + \frac{K}{8}(\zeta - c_1\eta)C_2\beta + \frac{K}{4\cdot 4!}(\zeta - c_1\eta)C_4\alpha_1 \right. \right. \\
& \qquad - \frac{K}{4\cdot 6!}(\zeta - c_1\eta)S_6 + \frac{K}{4\cdot 6!}(c_1\zeta + \eta)C_6 \\
& \qquad \left. \left. + \frac{K}{8}(c_1\zeta + \eta)S_2\beta + \frac{K}{4\cdot 4!}(c_1\zeta + \eta)S_4\alpha_1 \right) \right. \\
& \qquad - \beta\delta_2 - \frac{K}{2}(\zeta - c_1\eta)\left(-\frac{1}{6!}C_6 - \frac{1}{2}S_2\beta - \frac{1}{4!}S_4\alpha_1 \right) \\
& \qquad \left. - \frac{K}{2}(c_1\zeta + \eta)\left(\frac{1}{2}C_2\beta + \frac{1}{4!}C_4\alpha_1 - \frac{1}{6!}S_6 \right) \right] + \dots ,
\end{aligned}
\tag{26}
$$

where

$$
\begin{aligned}
C_n(\zeta,\eta) &= \frac{2\Gamma(n+1)}{(\zeta^2+\eta^2)^{(n+1)/2}} \cos\left[(n+1)\arctan(\eta/\zeta)\right] , \\
S_n(\zeta,\eta) &= \frac{2\Gamma(n+1)}{(\zeta^2+\eta^2)^{(n+1)/2}} \sin\left[(n+1)\arctan(\eta/\zeta)\right] ,
\end{aligned}
\tag{27}
$$

$$\begin{aligned}
\alpha_1 &= \frac{\delta_2}{2} - \frac{K}{8} S_2(\zeta - c_1\eta) + \frac{K}{8} C_2(c_1\zeta + \eta)\,, \\
\alpha_2 &= \frac{\delta_1}{2} + \frac{K}{8} C_2(\zeta - c_1\eta) + \frac{K}{8} S_2(c_1\zeta + \eta)\,,
\end{aligned} \tag{28}$$

and

$$\begin{aligned}
\beta &= \alpha_1\frac{\delta_1}{2} + \frac{K}{8}(\zeta - c_1\eta)C_2\alpha_1 + \frac{K}{8}(\eta + c_1\zeta)S_2\alpha_1 \\
&\quad -\frac{K}{4\cdot 24}(\zeta - c_1\eta)S_4 + \frac{K}{4\cdot 24}(\eta + c_1\zeta)C_4\,, \\
\beta_1 &= -\frac{3}{2}\alpha_1^2 - \delta_1\alpha_2 + \frac{\delta_2}{2}\alpha_1 + \frac{K}{32}(\zeta - c_1\eta)C_4 - \frac{K}{32}(\eta + c_1\zeta)S_4 \\
&\quad -\frac{K}{4}(\zeta - c_1\eta)C_2\alpha_2 - \frac{K}{4}(\eta + c_1\zeta)S_2\alpha_2 \\
&\quad -\frac{K}{8}(\zeta - c_1\eta)S_2\alpha_1 + \frac{K}{8}(\eta + c_1\zeta)C_2\alpha_1\,, \\
\beta_2 &= -\delta_1\alpha_2 + \delta_2\alpha_1 - \frac{K}{24}(\zeta - c_1\eta)C_4 - \frac{K}{24}(\eta + c_1\zeta)S_4 \\
&\quad -\frac{K}{4}(\zeta - c_1\eta)C_2\alpha_2 - \frac{K}{4}(\eta + c_1\zeta)S_2\alpha_2\,, \\
\beta_3 &= 3\alpha_1\alpha_2 - \frac{\delta_1}{2}\alpha_1 - \frac{5\delta_2}{2}\alpha_2 \\
&\quad -\frac{K}{8}(\zeta - c_1\eta)C_2\alpha_1 - \frac{K}{8}(\eta + c_1\zeta)S_2\alpha_1 \\
&\quad +\frac{K}{16}(\zeta - c_1\eta)S_4 - \frac{K}{16}(\eta + c_1\zeta)C_4 \\
&\quad +\frac{K}{8}(\zeta - c_1\eta)S_2\alpha_2 - \frac{K}{8}(\eta + c_1\zeta)C_2\alpha_2\,,
\end{aligned} \tag{29}$$

$$\begin{aligned}
\beta_4 &= -\frac{3}{2}\alpha_2^2 + \frac{K}{4\cdot 24}(\zeta - c_1\eta)C_4 + \frac{K}{4\cdot 24}(\eta + c_1\zeta)S_4 \\
&\quad +\frac{K}{8}(\zeta - c_1\eta)C_2\alpha_2 + \frac{K}{8}(\eta + c_1\zeta)S_2\alpha_2 + \frac{\delta_1}{2}\alpha_2\,.
\end{aligned} \tag{30}$$

Observe that the coefficients a_1, a_2, b_1, b_2, b_3, b_4, b_5 and g_1 are combinations of the independent parameters c_1, c_2, K, δ_1, δ_2 and θ (the latter is presented via ζ and η, see (12)). For the GL equation with *two* nonlocal terms, (13), which is in our focus, the phase equation is obtained by replacing

$$K(\zeta - c_1\eta)S_n \to K_1(\zeta_1 - c_{11}\eta_1)S_{n1} + K_2(\zeta_2 - c_{12}\eta_2)S_{n2}\,,$$

$$K(\eta + c_1\zeta)S_n \to K_1(\eta_1 + c_{11}\zeta_1)S_{n1} + K_2(\eta_2 + c_{12}\zeta_2)S_{n2}\,,$$

$$K(\zeta - c_1\eta)C_n \to K_1(\zeta_1 - c_{11}\eta_1)C_{n1} + K_2(\zeta_2 - c_{12}\eta_2)C_{n2}\,,$$

$$K(\eta + c_1\zeta)C_n \to K_1(\eta_1 + c_{11}\zeta_1)C_{n1} + K_2(\eta_2 + c_{12}\zeta_2)C_{n2}$$

$$(n = 2, 4, 6)$$

in (26) and also in the expressions for α_1 and α_2, (28), and for β, β_1, β_2, β_3 and β_4, (29)–(30). It was shown [9, 4] that the parameters K_1 and K_2 must satisfy the restriction

$$K_1 + K_2 < 1\,. \tag{31}$$

Another important condition that must be met is dissipative nature of the term $g_1\nabla^6\psi$, hence

$$g_1 > 0\,. \tag{32}$$

As we noted, equation (1) becomes a valid reduced form of (2) when $b_4 = -\varepsilon$, $b_5 = 1$ and $g_1 = 1$. In addition, all the lower-order terms preceding these three in the right-hand side of (2) must be negligible, which is achieved by assuming that the coefficients a_1, a_2, b_1, b_2 and b_3 are sufficiently small or even zero. Thus, these 5 coefficients alongside with the coefficient b_4 must satisfy the conditions of smallness — a total of 6 conditions.

We want to find out how narrow/wide is the area in parametric space of independent parameters within which (2) reduces to (1). We aim to determine a possibly larger piece of this area and, out of curiosity, compare it with the area leading to the KS equation. This is done in Section 2. Our second aim is to solve equation (1) numerically in two spatial dimensions in order to see whether complicated/irregular regimes may settle with time and what structure they have. We perform this in Section 3. Section 4 contains the conclusions.

2 Range of validity: numerical results

As an initial step we will demonstrate the existence of the values of the 9 independent parameters, θ_1, θ_2, c_{12}, c_{11}, c_2, K_1, K_2, δ_1 and δ_2, such that the 6 conditions of smallness are satisfied, namely that $b_4 = -\varepsilon$ (small number) and also a_1, a_2, b_1, b_2 and b_3 are sufficiently small or zero [9]. Additionally, the restrictions $g_1 > 0$, $\delta_1 > 0$, $K_1 + K_2 < 1$ must be satisfied.

Our numerical program, written in REDUCE, solves the equations stating that the coefficients a_1, a_2, b_1, b_2 and b_3 are equal to zero *exactly*. It is easy to verify that the softer conditions of the coefficients being slightly away from zero can always be achieved via tiny variations of the independent parameters from their values giving exactly zero values to the coefficients. Our program also computes the value of the parameter g_1 to see whether it satisfies the requirement $g_1 > 0$. The program works better when a small value $b_4 = -\varepsilon$ is arranged in the form of a product of one of the unknown parameters, for example K_1, and a small number: $b_4 = -K_1 \cdot 0.00001$. For the input values $\theta_1 = 1$, $\theta_2 = 2$, $c_{12} = 1$ the computed output (in rounded form) is

$$\delta_1 = 27\,, \quad K_1 = 49\,, \quad K_2 = -89$$

and

$$g_1 = 33\,.$$

See that all the restrictions are met, namely

$$g_1 > 0\,, \quad \delta_1 > 0\,, \quad K_1 + K_2 < 1\,. \tag{33}$$

Clearly we can make b_4 as close to zero as we wish. Thus, for the above values of the independent parameters the NEP equation is a valid truncation of the phase equation (2). Obviously, once there exists one valid point, it must be surrounded by a cloud of other valid points. We aim to determine a possibly wider range of the values of the parameters making the NEP equation valid. Similarly to the numerical example above, we execute the following procedure. We arbitrarily assign values to the 3 independent parameters θ_1, θ_2 and c_{12}. Using the program, we compute the values of the other 6 parameters from the list of 9. Finally, we inspect whether all the restrictions are met, and, based on the outcome, make a conclusion about whether or not a particular point in the 3D space $(\theta_1, \theta_2, c_{12})$ is a one where the NEP equation is valid. If at least one of restrictions (33) is violated, the NEP equation is not valid.

Approximately 87690 points in the 3D space were analysed and the result is shown in Fig. 1. All the points fall into three groups: the points where the NEP equation is valid, displayed as 'o', the points where the equation is not valid, displayed as '$*$', and the points, displayed as $\Box$, for which we were unable to make a conclusion about their validity because

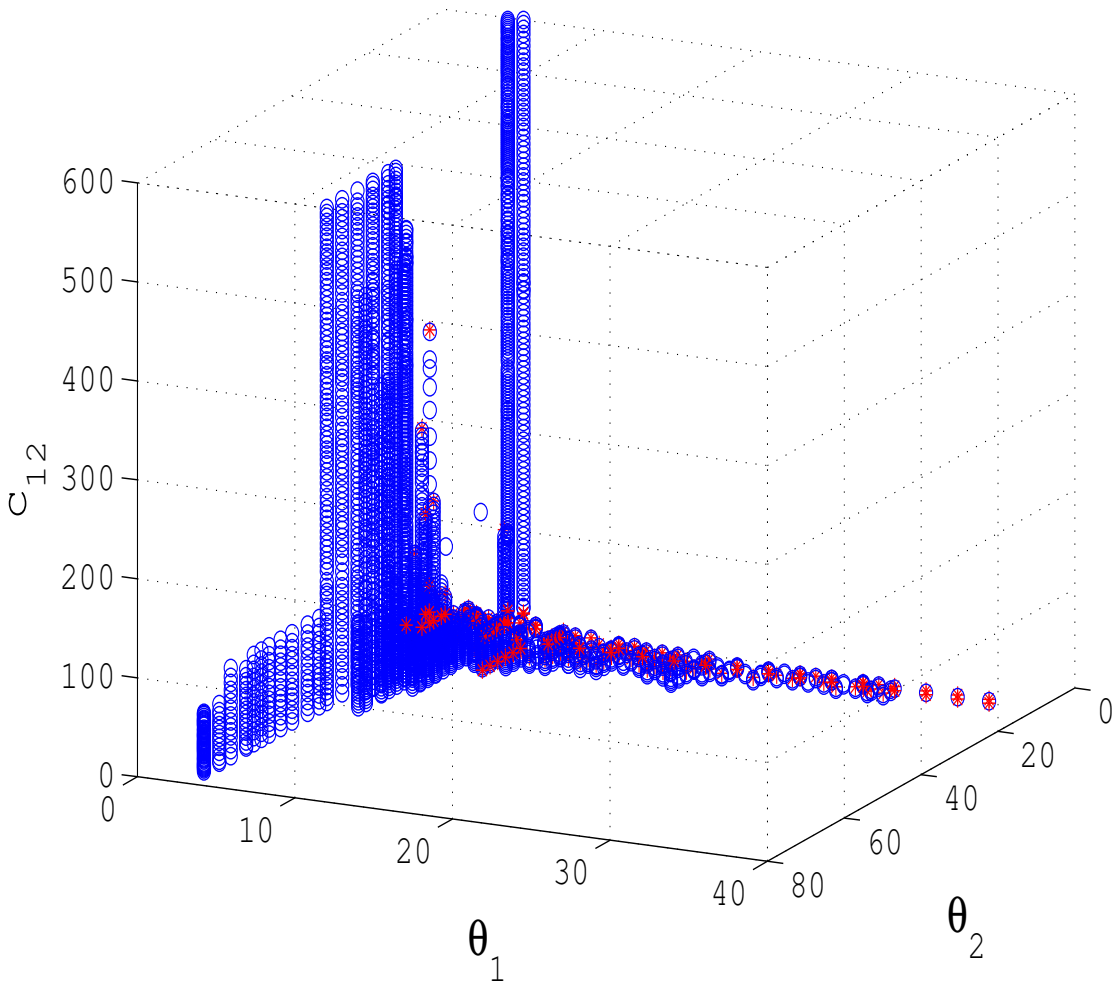

Figure 2: The area of validity of the NEP equation.

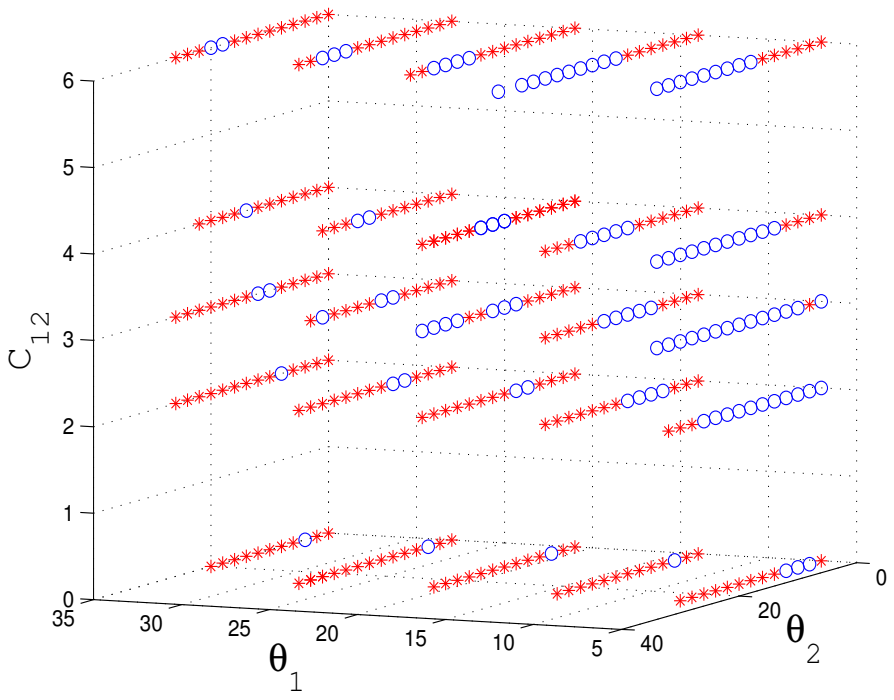

Figure 3: Valid and invalid points for the NEP equation along selected horizontal lines.

the computation took too long to finish. For brevity we will call the circles "valid" points and the stars "invalid" points. As is seen, the volume made of the valid points has a complicated shape. The circles 'o' may seem to form a continuous shape, however, at places they actually intermit with the stars. To show this fact, we scattered a small number of stars over the space, however, did not show all of them in order not to block the view of the circles. Bear in mind that the empty space around the circles is meant to be filled with stars (and squares). Note that the tall columns in Fig. 1 extend to infinity.

It is interesting to compare the validity areas for the NEP and Kuramoto-Sivashinsky equations. The KS equation (4) is relevant to many physical systems and can be deduced from (7)–(9) as well. Its validity area can be readily explored using our program after a simple adjustment. The KS equation is valid when only one condition on the coefficients is imposed, namely

$$a_1 = -\varepsilon < 0\,, \tag{34}$$

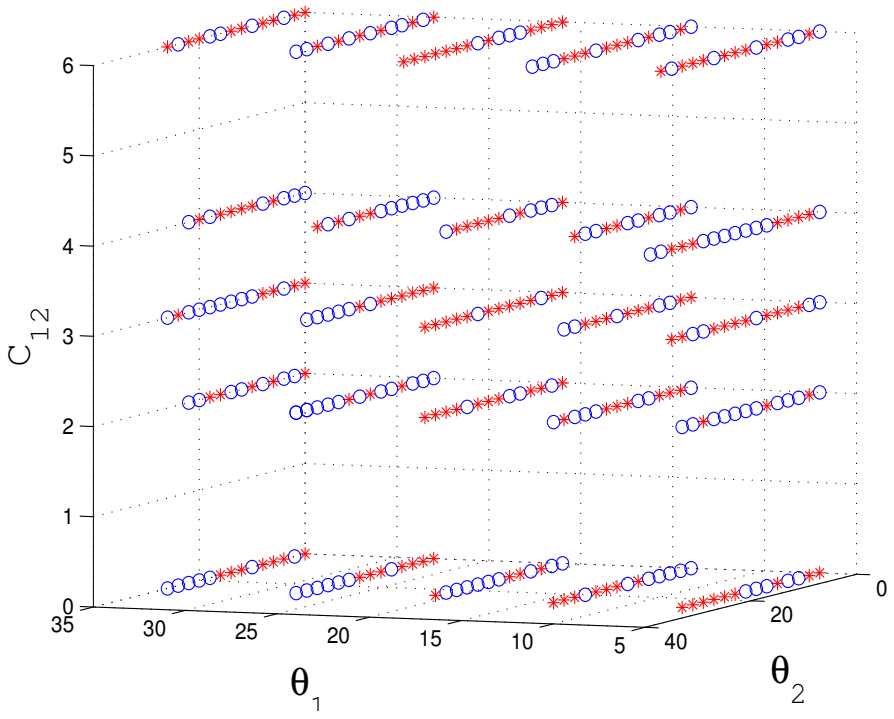

Figure 4: Valid and invalid points for the KS equation along selected horizontal lines.

and, additionally, the following restrictions are satisfied,

$$b_1 < 0\,, \quad \delta_1 > 0 \quad K_1 + K_2 < 1\,. \tag{35}$$

Out of the 9 independent parameters we have freedom to choose 8 so that the remaining 1 parameter is to be computed from equation (34). We choose this computed parameter to be δ_1. In analogy to the NEP case, we consider the 3D space $(\theta_1, \theta_2, c_{12})$. Let us select an arbitrary path in this space — a straight line. As we move from point to point along the line, the values of the 3 parameters change. For each point we assign values to the other 5 free parameters at our disposal, namely c_{11}, c_2, K_1, K_2 and δ_2. There is plenty of freedom in doing so, and our choice is to borrow these values from the NEP computational experiments executed at the same values of θ_1, θ_2 and c_{12}. The last step is to inspect signs of the computed parameters: if conditions (35) hold then the KS equation is valid at a given point. If at least one of these restrictions is not satisfied, then the KS equation is not valid at the point.

We opted to cut off a "box" in the 3D space $(\theta_1, \theta_2, c_{12})$ to capture considerable amount

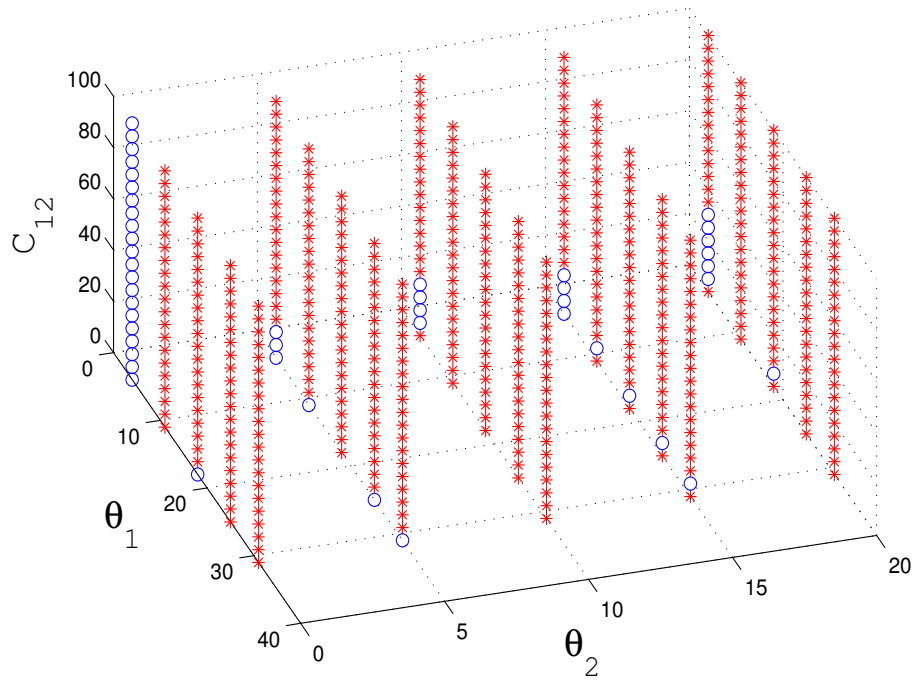

Figure 5: Valid and invalid points for the NEP equation along selected vertical lines.

of valid NEP points revealed by Fig. 1. Then we pierced the box by 25 straight lines forming a 5×5 grid. The lines uniformly fill the volume of the box. At all the point of the lines validity of the KS and NEP equations was tested. In the similar way we set up a grid of 25 vertical lines and analysed validity along them. The computational results are displayed in Fig. 2–5. For a quantitative comparison between the KS and NEP cases, we summed up the distances occupied by the KS valid points and, separately, NEP valid points, over all 25 horizontal lines and calculated the ratio ν =total NEP distance/total KS distance. The same was done for the vertical lines. The horizontal and vertical lines were analysed separately in this calculation in order not to mix the distances measured in units of c_{12} and those measured in units of θ_2. In both cases the ratio turned out to be less than one: $\nu_{vert} = 0.19$, $\nu_{horiz} = 0.85$. This shows that even in a box deliberately chosen to contain many valid NEP points, its total amount (the distance) is less than that for the KS equation. This seems to be a natural outcome since the KS equation imposes softer restriction on the coefficients of the phase equation. We note that the performed comparison is by no means exhaustive

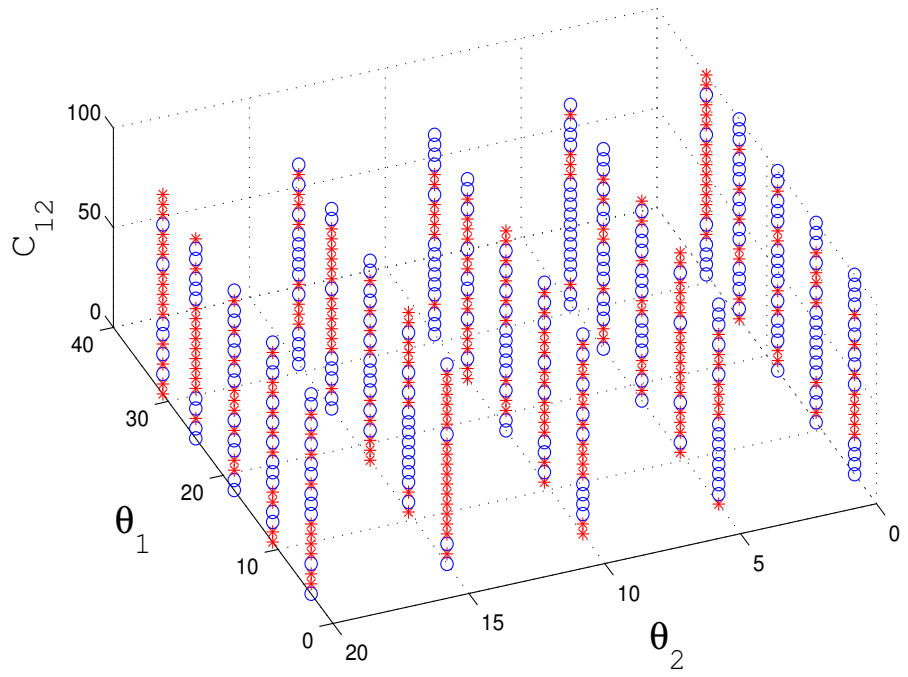

Figure 6: Valid and invalid points for the KS equation along selected vertical lines.

considering the many-dimensional (9D) space we deal with. We realize that (a) the KS area may be bounded or may spread to infinity in a given direction; and (b) many valid KS points may be located far away from the validity area of the NEP equation.

3 Forced and unforced dynamics

In this section we seek numerical and analytical solutions of equation (1) and its forced version, in two-dimensional space. In 2D equation (1) is written as

$$\begin{aligned} \partial_t u = & - A\left(\partial_x^2 u + \partial_y^2 u\right)\left[(\partial_x u)^2 + (\partial_y u)^2\right] \\ & + B\left[(\partial_x u)^4 + 2(\partial_x u)^2\,(\partial_y u)^2 + (\partial_y u)^4\right] \\ & + C\left(\partial_x^6 u + 3\partial_x^4\partial_y^2 u + 3\partial_x^2\partial_y^4 u + \partial_y^6 u\right) . \end{aligned} \tag{36}$$

Consider a square domain, $0 \le x, y \le L$. On the boundaries we stipulate zero value of the first, second, and third derivatives normal to the boundary,

$$\begin{aligned} &\partial_x u = 0\,, \quad \partial_x^2 u = 0\,, \quad \partial_x^3 u = 0 \quad \text{at} \quad x = 0 \;\text{ and }\; x = L\,, \\ &\partial_y u = 0\,, \quad \partial_y^2 u = 0\,, \quad \partial_y^3 u = 0 \quad \text{at} \quad y = 0 \;\text{ and }\; y = L\,. \end{aligned}$$

3.1 Derivation of the forced equation

So far we assumed that the rate c_2 was constant, both in time and space. Obviously this is an ideal situation while any real physical system is not perfectly uniform. It is interesting to explore the case when the rate c_2 varies in space; this assumption would represent a non-uniform distribution of the kinetics of the reacting system in space. In the ideal case of a constant rate c_2 the phase satisfies equation (16),

$$\partial_t \varphi = c_2 a^2 + \cdots = c_2(1 + \varepsilon_1^2 a_2 + \varepsilon_1^4 a_4 + \varepsilon_1^6 a_6 + \dots)^2 + \dots\,, \tag{37}$$

where the amplitude a is represented by the series (22) in small parameter ε_1 and the second set of dots denotes the terms which do not contain c_2. Now assume that c_2 is not constant is space (but still constant in time),

$$c_2 = c_2^{(0)} + \varepsilon_2 c_2^{(1)}(x, y)\,, \tag{38}$$

with $c_2^{(0)}$ being a constant and ε_2 being a new small parameter. Similarly to (18) we look for the phase in the form

$$\varphi(x, y, t) = c_2^{(0)} t + u(x, y, t)\,.$$

Then equation (37) becomes

$$\begin{aligned} c_2^{(0)} + \varepsilon_1^2 \partial_{t_1} u &= \left[c_2^{(0)} + \varepsilon_2 c_2^{(1)}\right](1 + \varepsilon_1^2 a_2 + \dots)^2 + \cdots = \left[c_2^{(0)} + \varepsilon_2 c_2^{(1)}\right](1 + 2\varepsilon_1^2 a_2 + \dots) + \dots \\ &= c_2^{(0)} + \varepsilon_2 c_2^{(1)} + \left\{\left[c_2^{(0)} + \varepsilon_2 c_2^{(1)}\right] 2\varepsilon_1^2 a_2 + \dots\right\} + \dots\,. \end{aligned} \tag{39}$$

The amplitude components a_n are separately expressed in terms of $\nabla_1 u$ from the amplitude equation (24) as we explained in the previous section. Substituting the expressions for a_n into (39), cancelling $c_2^{(0)}$ in both sides and performing some manipulations leads to

$$\begin{aligned} \varepsilon_1^2 \partial_{t_1} u = \varepsilon_2 c_2^{(1)} - \varepsilon_1^4 \nabla_1^2 u (\nabla_1 u)^2 \left\{\left[c_2^{(0)} + \varepsilon_2 c_2^{(1)}\right] 2\beta_3 + \dots\right\} \\ + \varepsilon_1^4 (\nabla_1 u)^4 \left\{\left[c_2^{(0)} + \varepsilon_2 c_2^{(1)}\right] 2\beta_4 + \dots\right\} + \varepsilon_1^6 \nabla_1^6 u \left\{\left[c_2^{(0)} + \varepsilon_2 c_2^{(1)}\right] \delta_1 \beta + \dots\right\} + \dots\,, \end{aligned} \tag{40}$$

where δ_1, β_n and β are the parameters composed of the original parameters of the physical system. Note that the lower-order terms in ∇_1, carried by a_2 and a_4, vanished because the resulting factors in front of them are made zero. This is done by the appropriate choice of the magnitudes of the original parameters, as we mentioned in the previous section. To evaluate the order of the small parameter ε_2 we need to take into consideration that all the terms in (40) must have the same order of magnitude. Therefore, evaluating quantities by their absolute value, we have

$$\varepsilon_2 c_2^{(1)} \sim b_4 \nabla^2 u \left(\nabla u\right)^2 . \tag{41}$$

By the definition of ε and in view of the connection (19),

$$b_4 = \varepsilon = \varepsilon_1^{2/3} .$$

The scales of the length, L, and phase departure, U, are found in (6),

$$u \sim U \sim \varepsilon = \varepsilon_1^{2/3} , \quad \nabla \sim L^{-1} \sim \varepsilon_1 ,$$

consequently,

$$b_4 \nabla^2 u \left(\nabla u\right)^2 \sim b_4 \frac{U^3}{L^4} \sim \varepsilon_1^{20/3} .$$

Since the parameter ε_2 is introduced presuming $c_2^{(1)} \sim 1$, then, using (41), we determine

$$\varepsilon_2 = \varepsilon_1^{20/3} .$$

Finally, neglecting $\varepsilon_2 c_2^{(1)}$ inside the square brackets in (40) in comparison to $c_2^{(0)}$ and returning to the unscaled operators $\nabla = \varepsilon_1 \nabla_1$ and $\partial_t = \varepsilon_1^2 \partial_{t_1}$ we arrive at the forced equation

$$\partial_t u = -A \nabla^2 u (\nabla u)^2 + B (\nabla u)^4 + C \nabla^6 u + f(x, y) , \tag{42}$$

where the force term, $f(x, y)$, is in fact the scaled rate $\varepsilon_2 c_2^{(1)}(x, y)$ from (40).

Our interest in the forced equation (42) is three-fold: (1) explore the effects of slow variations of the kinetics in space (the nonuniformity of the reacting medium), (2) construct exact solutions of the forced equation and numerically investigate their stability, (3) test the numerical code by comparing the numerical solutions with the exact solutions.

3.2 Exact solutions of the forced equation. Testing the numerical code

We wrote a Matlab numerical code to solve equation (42). The spatial part of the equation is discretized using central finite differences and the resulting system of ordinary differential equations is integrated in time by the DAE2 solver [11]. The solver ensures a good accuracy, nevertheless we carried out our own tests as described further in this section. The idea for the tests was to adopt the force function $f(x, y, t)$ in special forms in order to ensure that the forced equation (42) allows exact (a) stationary or (b) oscillating solution of our choice. It was important that the solutions were stable otherwise it would not be possible to obtain them in the course of our nonstationary numerical experiments. Here is a simple example where a desired solution is unstable. Consider the ordinary differential equation

$$dF/dt = F\,.$$

and let us wish that the forced equation

$$dF/dt = F + F_1 \tag{43}$$

has the exact solution $F_0 = 1$. According to (43) we choose $F_1 = dF_0/dt - F_0 = -1$. It is easy to see, however, that the solution $F_0 = 1$ is unstable. For equation (42) we would not know apriori whether our chosen solution is stable or not, but if it is stable, our numerical code should be capable of reproducing it. If it proves unstable, we would need to choose a different solution. With this in mind, we conducted two tests. For the first test we desired, as in the above simple example, that the forced equation had a stationary solution. Of course the solution needs to be nontrivial (non-constant) is space and must satisfy the boundary conditions. For the second test we created a nonstationary solution by multiplying the stationary one by an oscillating function of time. The two cases are represented by the single formula

$$u \equiv v(x, y, t) = M[1 + k\sin(\omega t)]\, x^4(x - L)^4 y^4(y - L)^4\,, \tag{44}$$

where $k = 0$ gives the stationary solution and $k \neq 0$ the nonstationary one. Write equation (42) as

$$\partial_t u = \mathrm{RHS} + f(x, y, t)\,, \tag{45}$$

where RHS stands for the right-hand side of (1). Substituting (44) into (45) we get

$$f(x, y, t) = \partial_t v(x, y, t) - \mathrm{RHS}[v(x, y, t)]\,. \tag{46}$$

giving

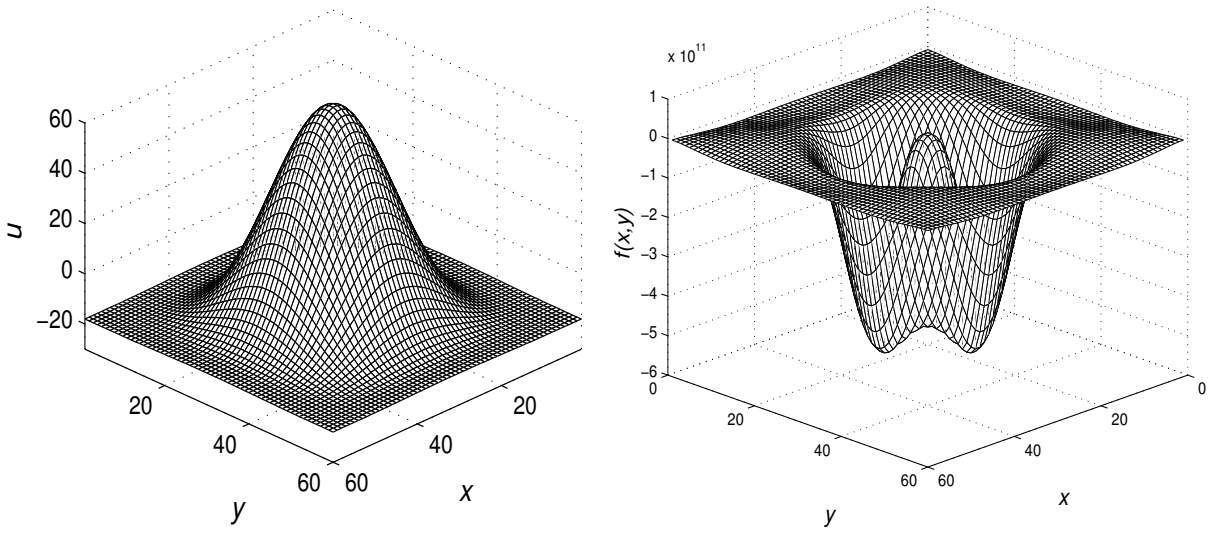

Figure 7: The exact solution (44) ($k = 0$) [left] and the force function (46) [right]. $M = 1.3 \cdot 10^{13}$, $L = 0.4$. The axes show grid points.

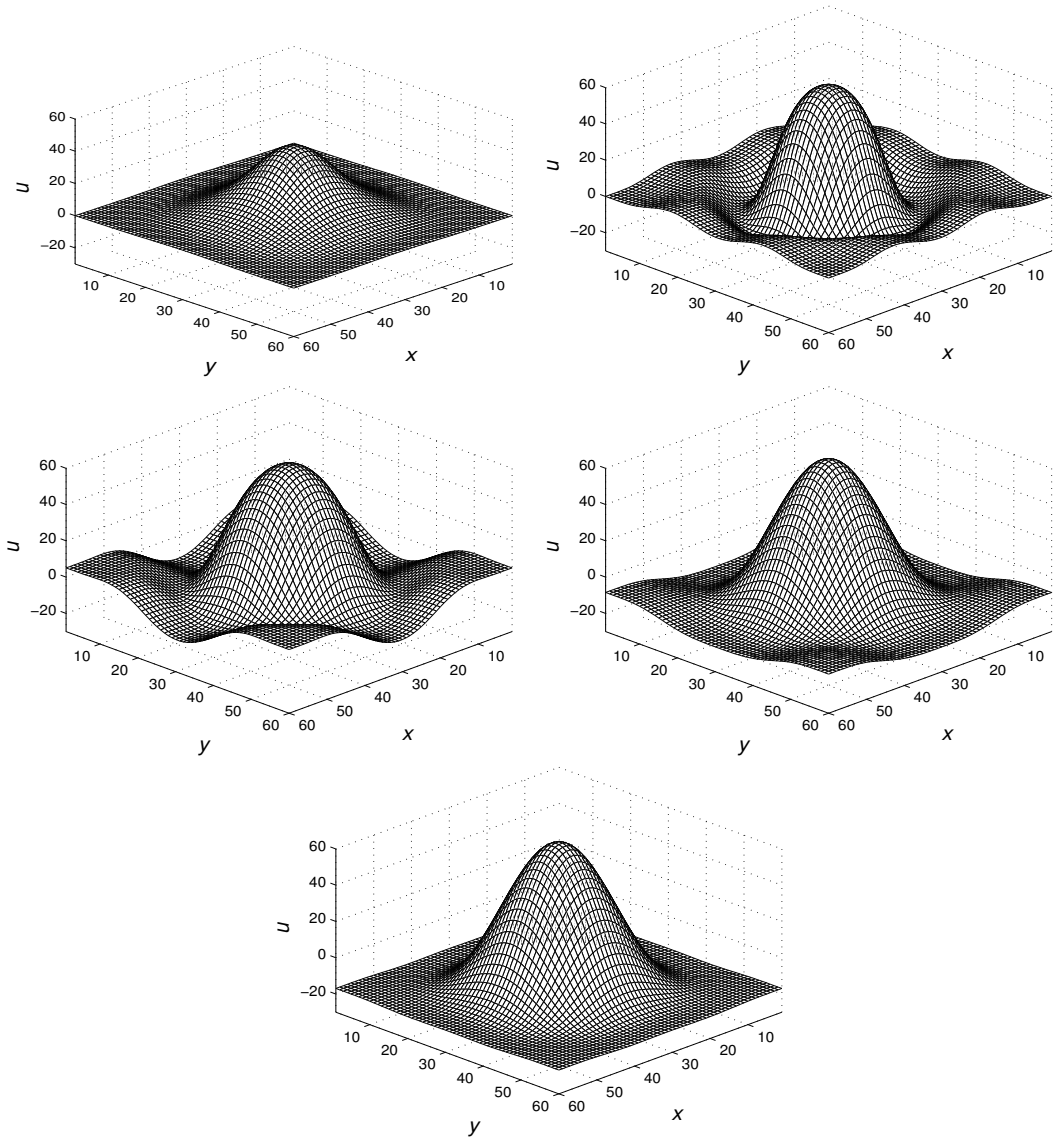

Figure 8: Evolution of the numerical solution of (42) towards the stationary regime. $t = 1.1 \cdot 10^{-11},\ 1.24 \cdot 10^{-10},\ 1.735 \cdot 10^{-10},\ 10.0 \cdot 10^{-10},\ 20.0 \cdot 10^{-10}$. The equation coefficients $A = 10$, $B = C = 1$. The domain size $L = 0.4$.

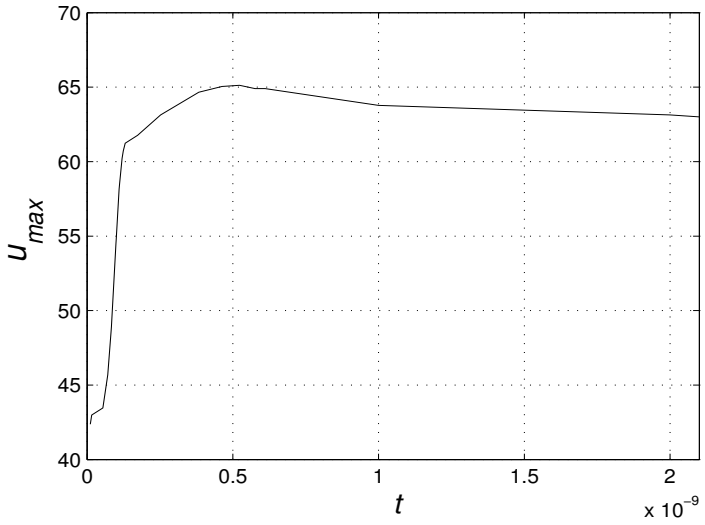

Figure 9: Settling of the maximum of u in the 60×60-grid experiment.

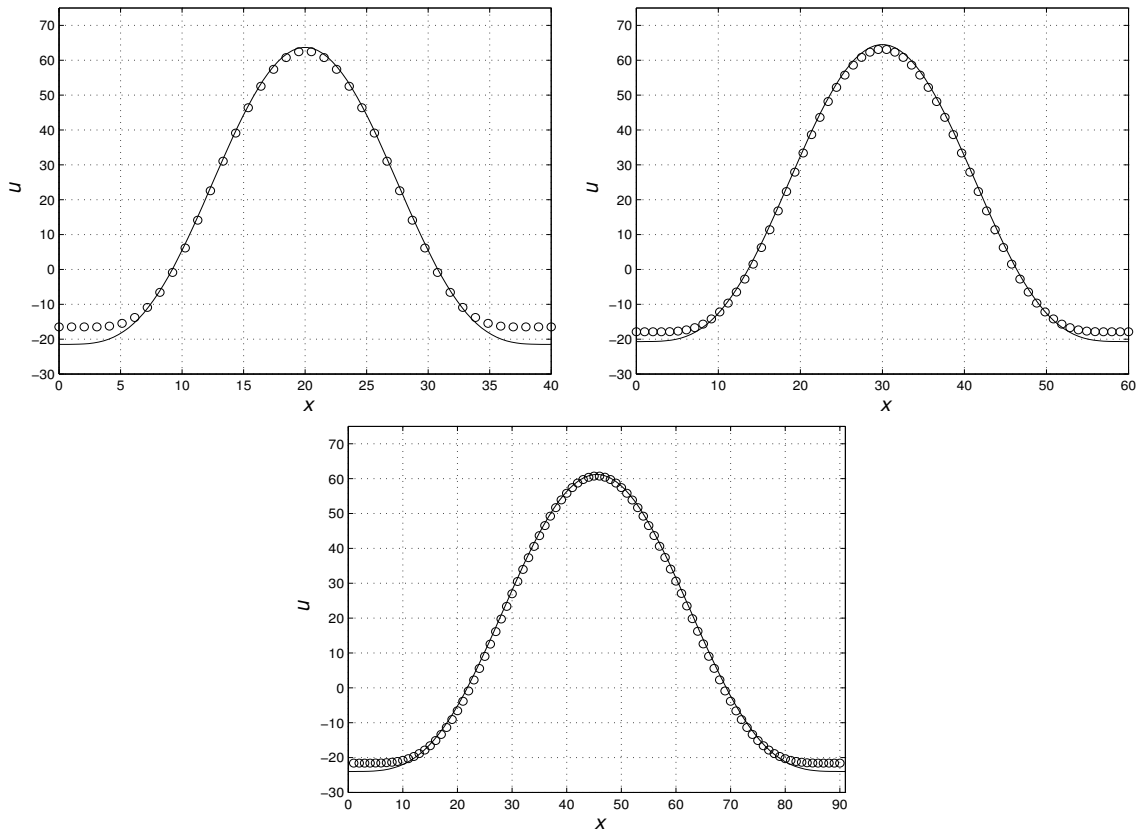

Figure 10: The exact solution (44) and settled numerical solution (circles) at $t = 20.0 \cdot 10^{-10}$ for 40×40, 60×60 and 90×90-grid experiments ($u(x, y_0)$ at $y_0 = 0.2$ (grid points 20, 30 and 45 respectively)).

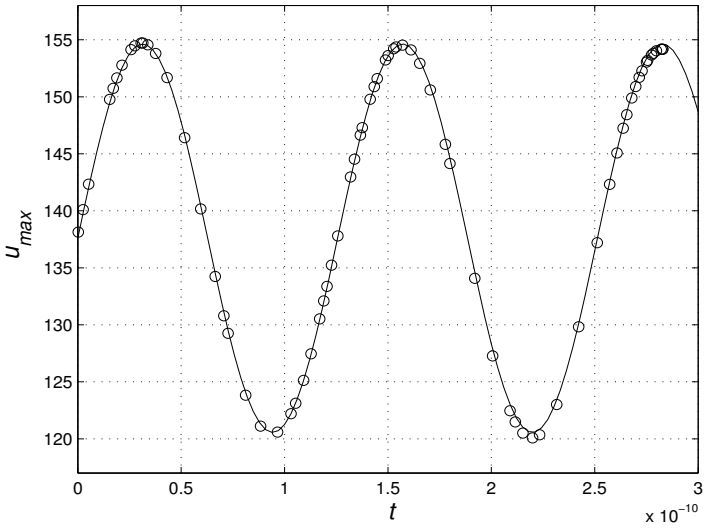

Figure 11: The exact and numerical (circles) solutions for the oscillatory regime.

$$f(x,y,t) = Mk\omega\cos(\omega t)\,x^4(x-L)^4y^4(y-L)^4$$

$$\begin{aligned}
&- cM[1+k\sin(\omega t)]\left\{\left[4320(x-L)^2+11520x(x-L)+4320x^2\right]y^4(y-L)^4\right.\\
&+3\left[24(x-L)^4+384x(x-L)^3+864x^2(x-L)^2+384x^3(x-L)+24x^4\right]\\
&\times\left[12y^2(y-L)^4+32y^3(y-L)^3+12y^4(y-L)^2\right]\\
&+3\left[24(y-L)^4+384y(y-L)^3+864y^2(y-L)^2+384y^3(y-L)+24y^4\right]\\
&\times\left[12x^2(x-L)^4+32x^3(x-L)^3+12x^4(x-L)^2\right]\\
&\left.+\left[4320(y-L)^2+11520y(y-L)+4320y^2\right]x^4(x-L)^4\right\}
\end{aligned}$$

$$\begin{aligned}
&+ gM^3[1+k\sin(\omega t)]^3\left\{\left[12x^2(x-L)^4+32x^3(x-L)^3+12x^4(x-L)^2\right]y^4(y-L)^4\right.\\
&+\left.\left[12y^2(y-L)^4+32y^3(y-L)^3+12y^4(y-L)^2\right]x^4(x-L)^4\right\}\\
&\times\left\{\left[4x^3(x-L)^4+4x^4(x-L)^3\right]^2y^8(y-L)^8\right.\\
&+\left.\left[4y^3(y-L)^4+4y^4(y-L)^3\right]^2x^8(x-L)^8\right\}
\end{aligned}$$

$$
\begin{aligned}
&- bM^4[1+k\sin(\omega t)]^4 \left\{ \left[4x^3(x-L)^4 + 4x^4(x-L)^3\right]^4 y^{16}(y-L)^{16} \right. \\
&+ 2\left[4x^3(x-L)^4 + 4x^4(x-L)^3\right]^2 y^8(y-L)^8 \\
&\times \left[4y^3(y-L)^4 + 4y^4(y-L)^3\right]^2 x^8(x-L)^8 \\
&\left. + \left[4y^3(y-L)^4 + 4y^4(y-L)^3\right]^4 x^{16}(x-L)^{16} \right\} .
\end{aligned}
\tag{47}
$$

Consider the stationary case first ($k = 0$). The shapes of the exact solution (44) and the corresponding force function are shown in Fig. 7. The numerical solution, as it evolves from the initial condition, is given in Fig. 8. At the initial moment the function was chosen to have a similar shape to (44) (with $k = 0$), only with half the height. Note the large time interval between the second and third snapshots. The time step $\Delta t = 5 \cdot 10^{-13}$. See that the numerical solution gradually increases in height and adjusts its peripheral parts. We see a clear resemblance between the numerical and exact solutions. A more precise evidence of their closeness is given by Fig. 9; it shows the evolution of the maximum of u, that is the value of the function in the centre of the domain. Stability of the solution is proved by the nonstationary experiment. There is a slight vertical drift of the nearly horizontal curve because the stationary solution is only *neutrally* stable. As a result, equation (45) allows a family of solutions $u = v(x, y, t) + C$ with different constants C. The inevitable numerical mismatch between the exact force $f(x, y, t)$ and discretized RHS in (45) causes the slow drift from one stationary solution to another. Fig. 10 compares the settled numerical and exact profiles along the centre of the domain, $y = 0.2$, demonstrating a good agreement except near the edges. Expectedly, the agreement improves for finer grids. Our second test reproduced the oscillating solution (44) with $k = 0.2$, $\omega = 10^{11}$ and the same values for the other parameters (the time step $\Delta t = 2 \cdot 10^{-14}$). Fig. 11 displays the evolution of the maximum of u. See that the numerical and exact solutions are close and, again, there is a slow drift due to the neutral nature of stability.

3.3 Intermittent and irregular dynamics under the unforced equation

In this section we consider the original unforced equation (1). We present just one numerical experiment, which took a long time (months) to run in real terms. The reason was the

large size of the domain that we chose aiming to provide enough space for the dissipative structures to form and interact with each other. An inevitable price for the choice was that many gridpoints were required to spatially resolve the dissipative structures. Hopefully this would lead (and actually did) to the complicated irregular dynamics. Small domains are less interesting as they would result in a flat motionless u-field. To investigate the onset of chaos at transitional domain sizes – from small to large – is an interesting task but at this stage we leave it for the future because of the computer limitations.

We present a series of snapshots showing the numerical experiment with the domain size $L = 2$. A 60×60 grid is chosen as a compromise between accuracy and speed of computation. The snapshots are shown in pairs: the function itself at a specified moment of time and, next to it, the corresponding plot of the excitation term, $-A\nabla^2 u(\nabla u)^2$. Recall that it is this term that is responsible for the energy release in the system, hence it indicates the area where the "action" is actually occurring at a given moment. The initial condition was a single narrow peak sitting on the plateau $u \equiv 0$ (top Fig. 12). The snapshots are complemented by the graph of the integral excitation, Fig. 17,

$$\int_0^L \int_0^L \left| A\nabla^2 u(\nabla u)^2 \right| \, dxdy \tag{48}$$

as a measure of the intensity of the dynamics. After an initial period of violent dynamics (not shown) the surface becomes smooth as shown by the second-from-the-top snapshot in Fig. 12. Gradually, after the relatively calm evolution during $t < 450 \cdot 10^{-9}$ the dynamics build up and remain intensive for $450 \cdot 10^{-9} < t < 900 \cdot 10^{-9}$. Then the motion slows down before picking up again around $t \sim 1500 \cdot 10^{-9}$. It appears we have recorded a cycle of the dynamics, slow motion — burst — slow motion, and the beginning of the next cycle. Irregularity of the dynamics within the cycle is demonstrated by Fig. 18. It shows the positions of the absolute maximum of the excitation term on the (x, y)-plane. In addition, Fig. 19 also shows the positions of the second-largest maximum of the excitation.

The way the shape of the function $u(x, y, t)$ looks and moves is remarkably different to a typical behaviour of a *linearly* excited system, such as the Kuramoto-Sivashinsky equation and Nikolaevskii equation. Under the boundary and initial conditions similar to those of our experiments, the linearly excited models produce dissipative structures simultaneously emerging (with certain dominant wavelengths) all over the available spatial domain. This

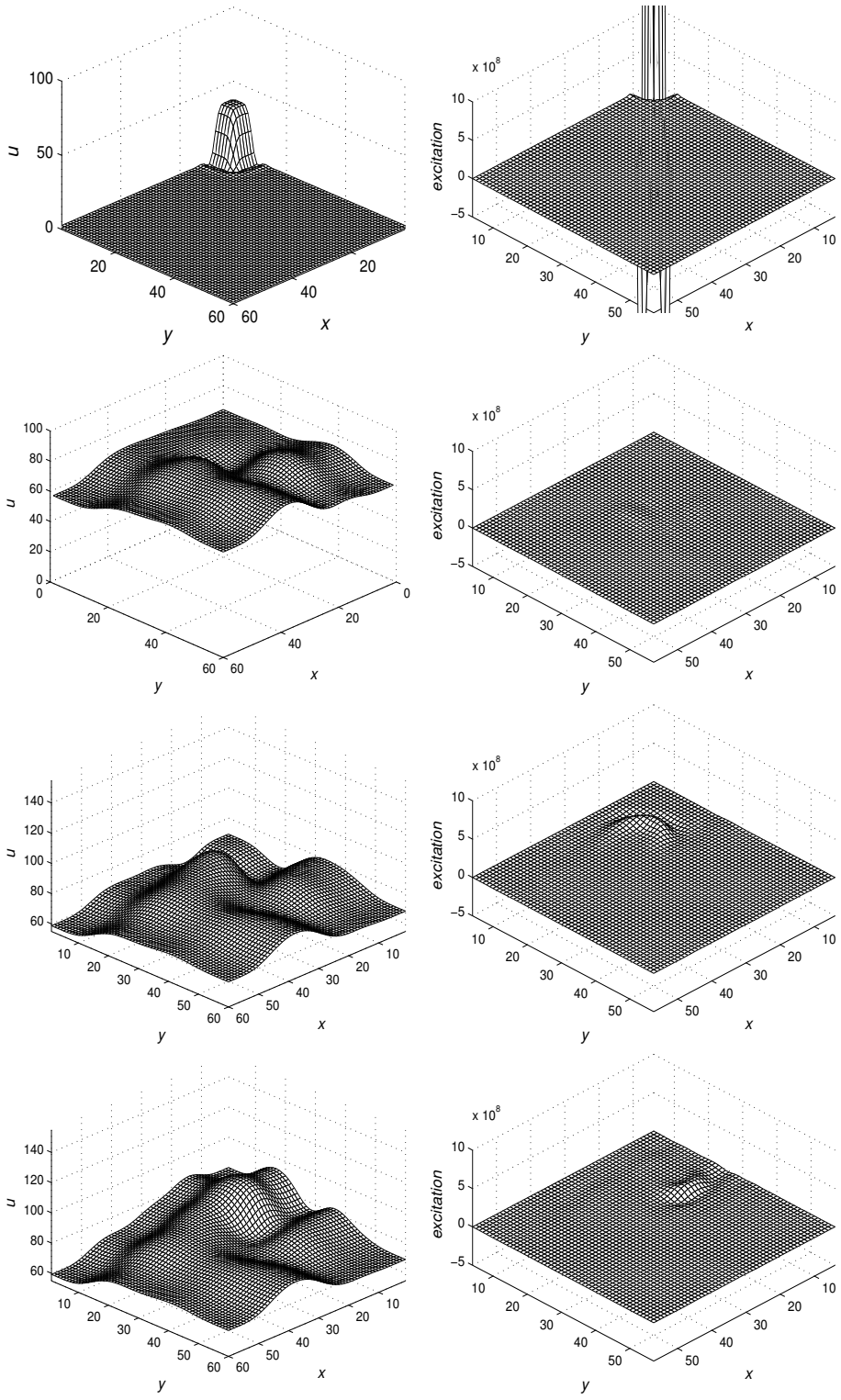

Figure 12: $t = t_0$, $9 \cdot 10^{-9}$, $150 \cdot 10^{-9}$, $225 \cdot 10^{-9}$.

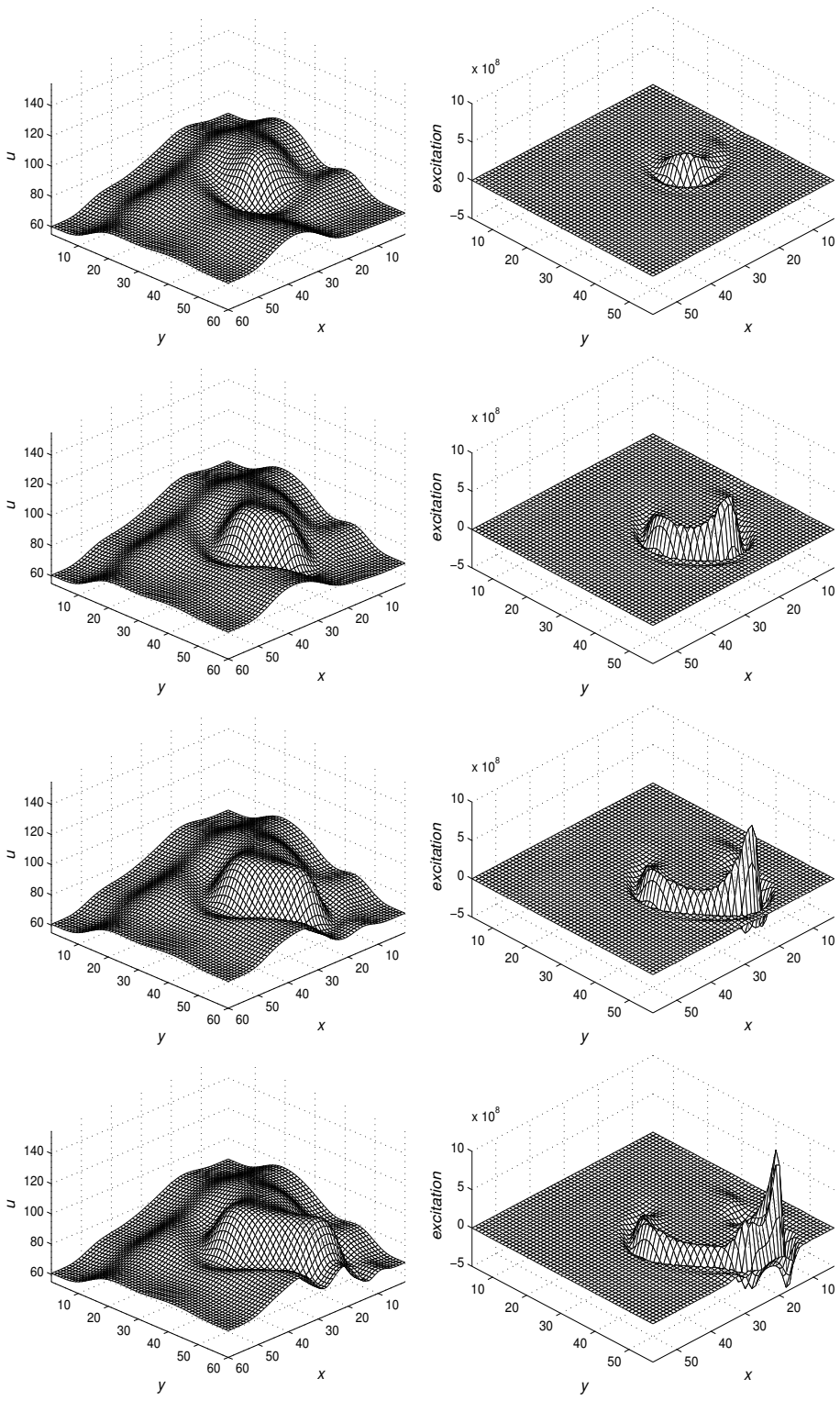

Figure 13: $t = 462 \cdot 10^{-9}$, $510 \cdot 10^{-9}$, $541.5 \cdot 10^{-9}$, $552 \cdot 10^{-9}$.

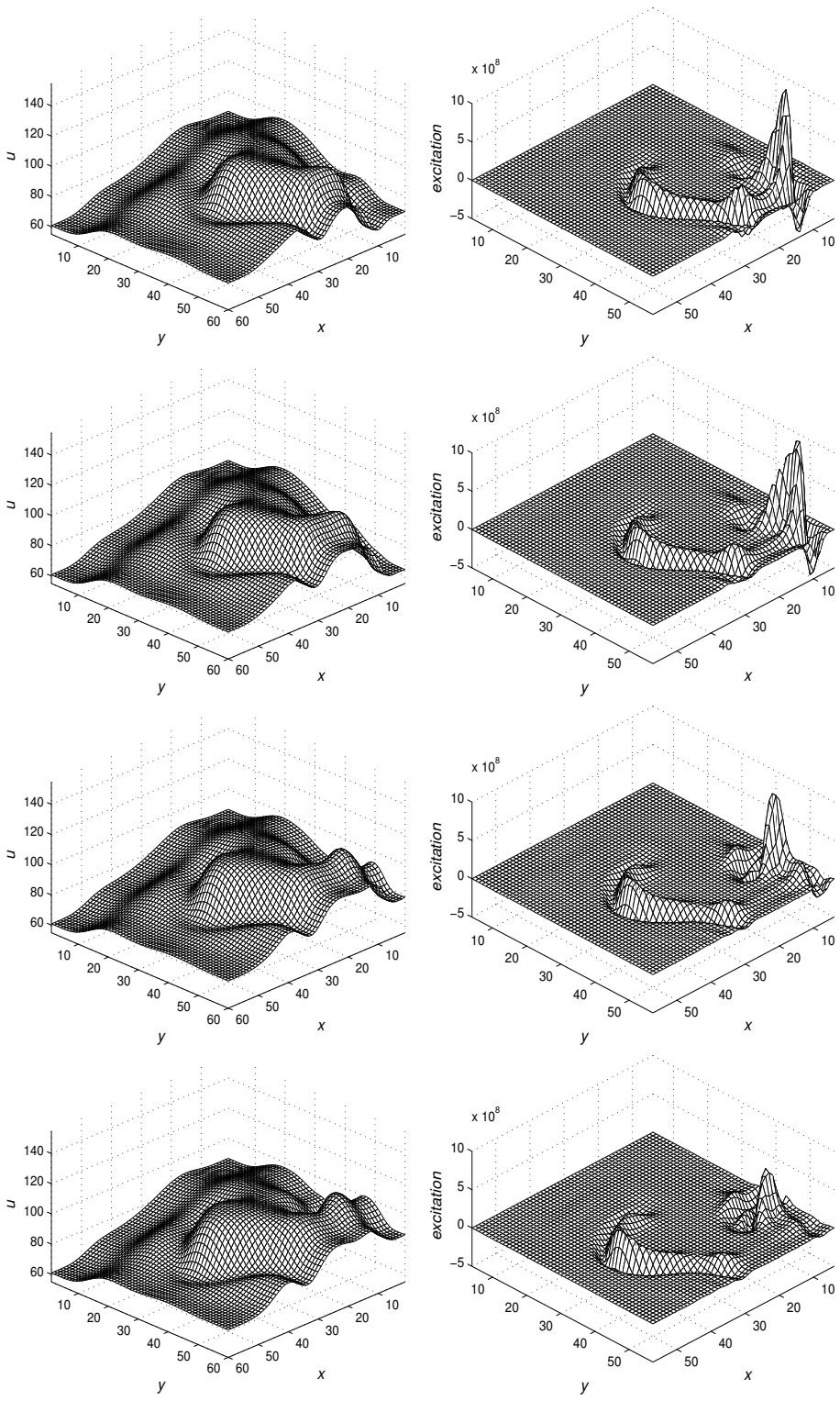

Figure 14: $t = 558 \cdot 10^{-9}$, $570 \cdot 10^{-9}$, $588 \cdot 10^{-9}$, $609 \cdot 10^{-9}$.

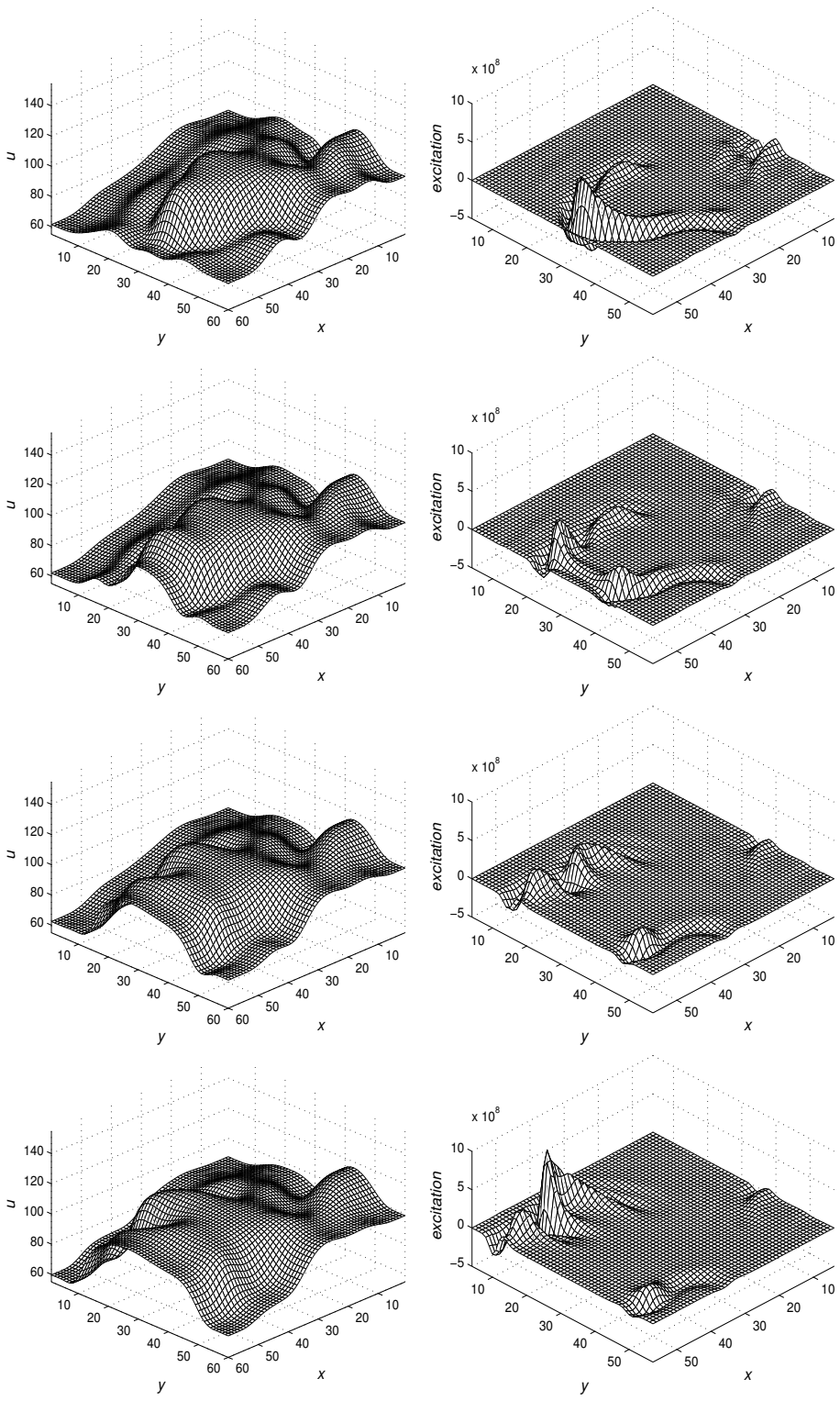

Figure 15: $t = 651 \cdot 10^{-9}$, $679.5 \cdot 10^{-9}$, $738 \cdot 10^{-9}$, $769.5 \cdot 10^{-9}$.

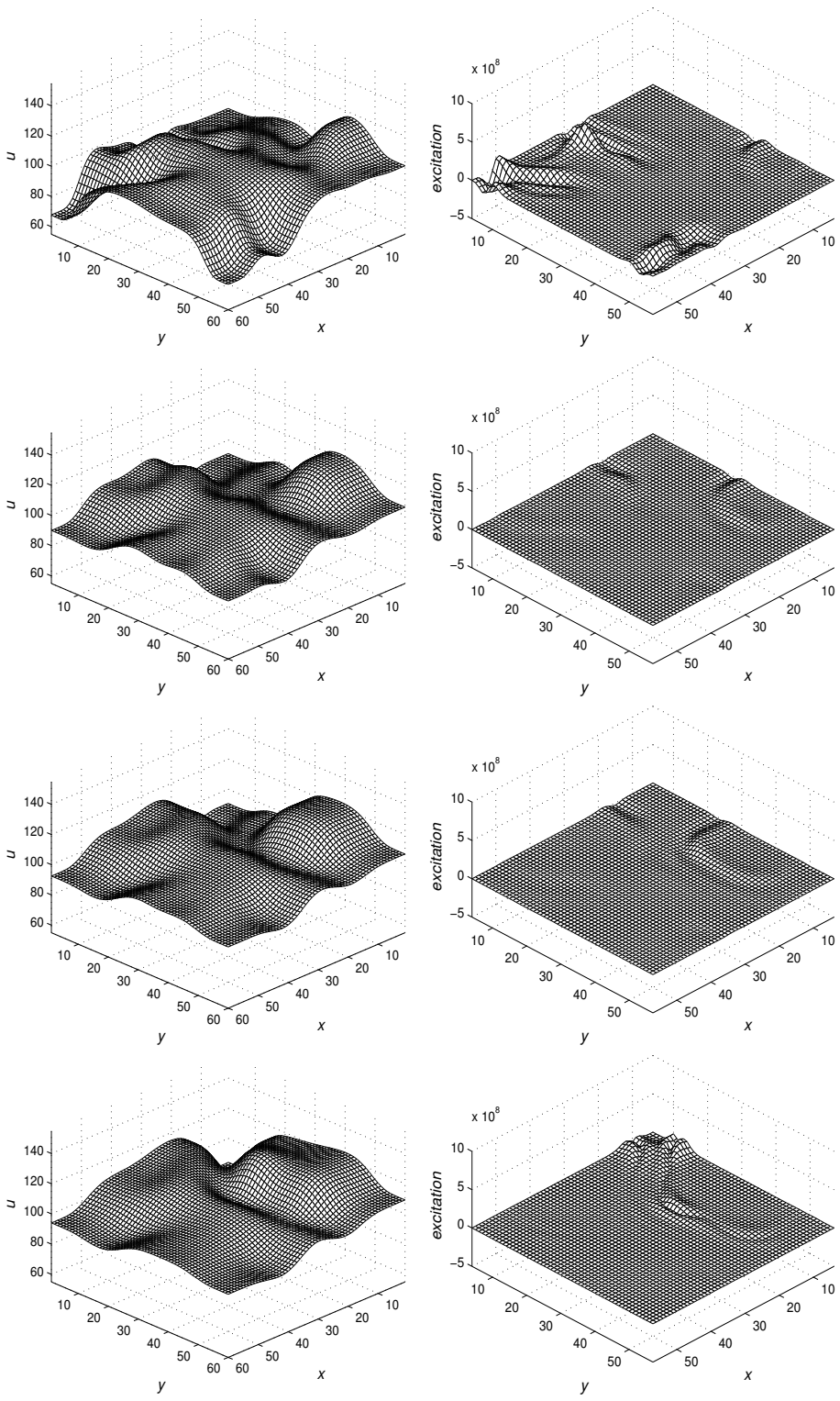

Figure 16: $t = 822 \cdot 10^{-9}$, $1281 \cdot 10^{-9}$, $1519.5 \cdot 10^{-9}$, $1873.5 \cdot 10^{-9}$.

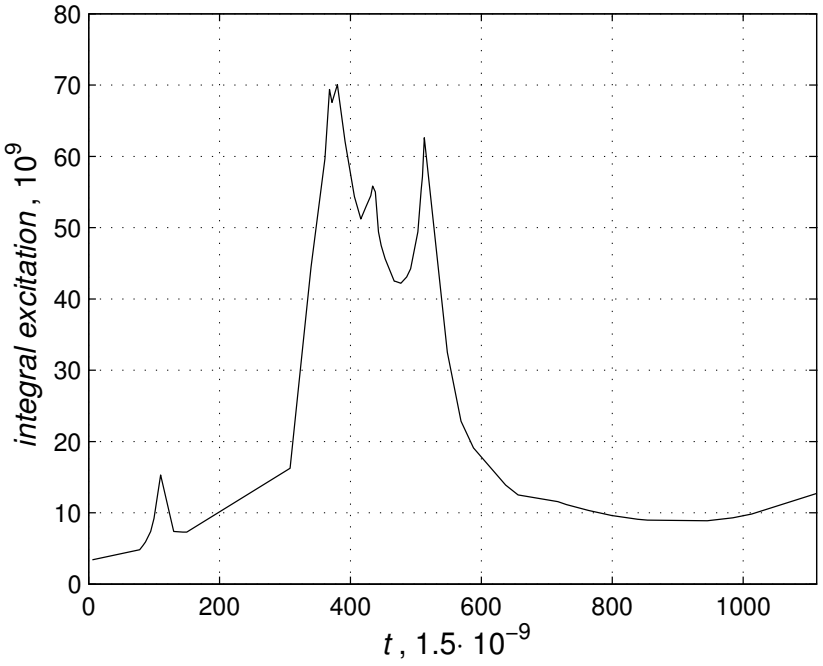

Figure 17: Integral of the absolute excitation.

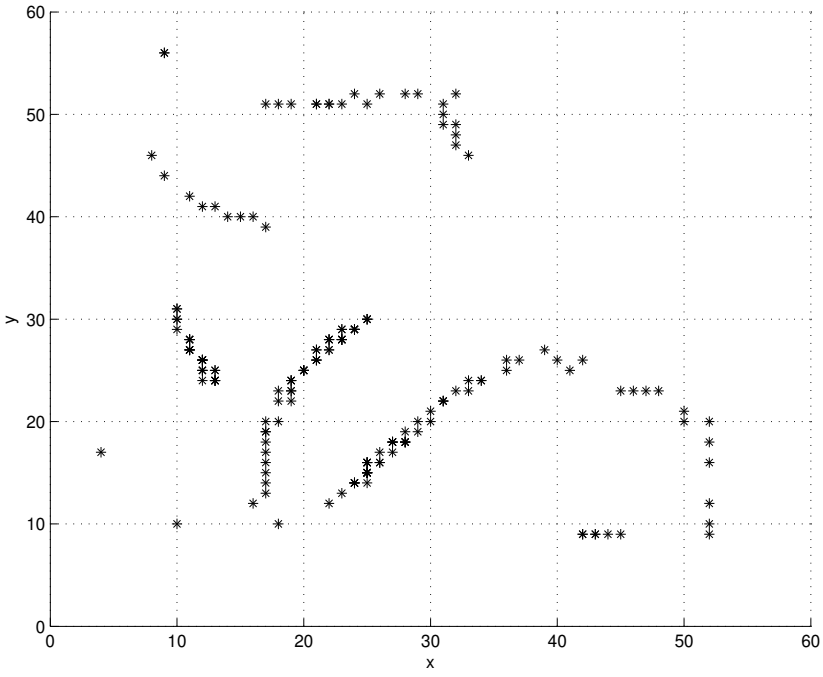

Figure 18: The positions of the global maximum of the excitation at different moments.

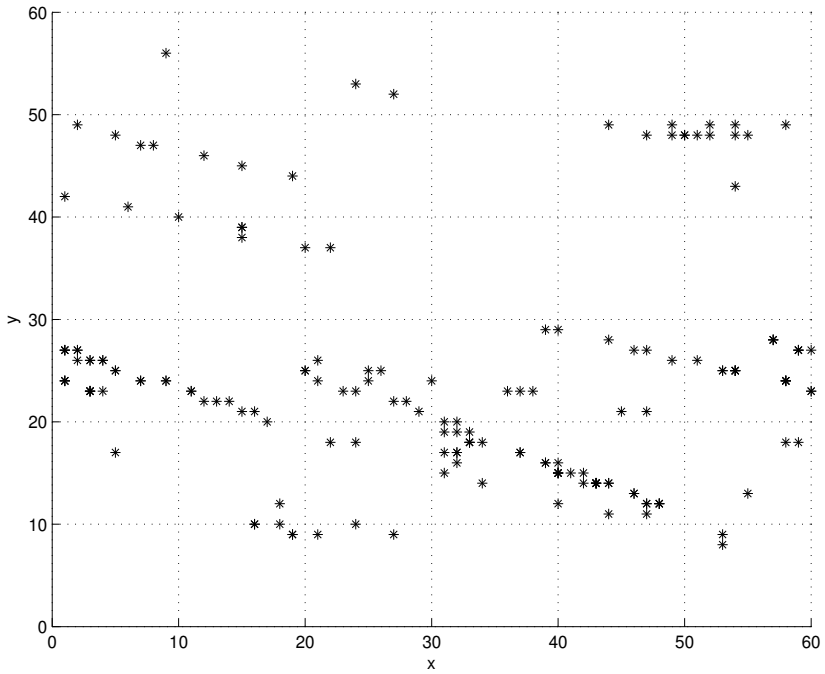

Figure 19: The positions of the second-largest maximum of the excitation at different moments.

is because any flat fragment of the u-field quickly transforms into a lumpy shape by the linear instability mechanism. By contrast, in our case, characterised by the linear stability, significant portions of the u-field remain almost flat until the signal arrives to them from other locations. The maximum of the excitation, which is concentrated on the steepest slopes, moves like a worm digging its way in predominantly lateral direction. Having travelled over the domain, the worm sooner or later returns to its earlier (x, y)-location. Qualitatively this is the same type of behaviour as the spinning combustion waves, only irregular.

4 Conclusions

The work consists of two parts. In the first part we evaluated the area of validity of the nonlinearly excited phase equation in parametric space for a system of nonlocally coupled oscillators. We compared the validity areas for the NEP and KS equations within the same system. The 8D subspace of the 9D space of independent parameters was pierced by a set of lines. The 8 parameters spanning the subspace were chosen to be θ_1, θ_2, c_{12}, c_{11}, c_2, K_1,

K_2 and δ_2. It is only possible to graphically display three (or fewer) dimensions, for example θ_1, θ_2 and c_{12}, which was done. The lines in the 8D subspace are identical for both the NEP and KS equations. At each point on the lines each equation is either valid or invalid and sometimes our result was inconclusive. We found that the NEP equation has a sizable range of validity, yet narrower than that for the KS equation. This can be explained by the stricter conditions required by the NEP equation. We derived the forced version of the NEP equation addressing nonuniformity of the reacting medium in space. Selected exact solutions of this version were constructed. Stability of the solutions was demonstrated by the numerical experiments. Comparison of the exact and numerical solutions demonstrates satisfactory performance of the numerical code. For the unforced version of the equation, we revealed periods of fast irregular dynamics intermitting with stages of slow evolution.

References

[1] G.I. Sivashinsky, Nonlinear analysis of hydrodynamical instability in laminar flames, Acta Astronaut. 4 (1977) 1177–1206.

[2] A.G. Merzhanov and E.N. Rumanov, Physics of reaction waves, Rev. Mod. Phys. 71 (1999) 1173–1211.

[3] Y. Kuramoto and T. Tsuzuki, Persistent propagation of concentration waves in dissipative media far from thermal equilibrium, Progr. Theor. Phys. 55 (1976) 356–369.

[4] D. Tanaka and Y. Kuramoto, Complex Ginzburg-Landau equation with nonlocal coupling, Phys. Rev. E 68 (2003) 026219.

[5] D. Tanaka, Chemical turbulence equivalent to Nikolaevskii turbulence, Phys. Rev. E 70 (2004) 015202(R).

[6] V.N. Nikolaevskii, in Recent Advances in Engineering Science, edited by S.L. Koh, C.G. Speciale, Lecture Notes in Engineering, 39 Berlin: Springer, 1989, 210.

[7] D.V. Strunin, Autosoliton model of the spinning fronts of reaction, IMA J. Appl. Math. 63 (1999) 163–177.

[8] D.V. Strunin, Nonlinear instability in generalized nonlinear phase diffusion equation, Progr. Theor. Phys. Suppl. N 150 (2003) 444–448.

[9] D.V. Strunin, Phase equation with nonlinear excitation for nonlocally coupled oscillators, Physica D: Nonlinear Phenomena 238 (2009) 1909–1916.

[10] D.V. Strunin, A.G. Strunina, E.N. Rumanov and A.G. Merzhanov, Chaotic reaction waves with fast diffusion of activator, Phys. Lett. A 192 (1994) 361–363.

[11] http://www.mathworks.com/matlabcentral/fileexchange/28-differential-algebraic-equation-solvers